Quantum Statistical Features of the Mth Nonlinear Coherent States within the F-Deformed Jaynes-Cummings Model

Seyyed Majid Heydari[a], Akbar Jafari[a,*], and Omid Abbasi[b]

[a]Department of Physics, Urmia University, Urmia, Iran
[b]Department of Physics, Faculty of Computer Engineering, Islamic Azad University, Najafabad Branch, Najafabad, Iran

Corresponding author email: <u>a.jafari@urmia.ac.ir</u>

ABSTRACT— Recently, we introduced the Mth nonlinear coherent state (MNCS), obtained by applying M times the number operator on the nonlinear coherent states (NCSs). Studying the interaction of such states with an atom is of great importance due to their notable nonclassical features. In this study, relying on the f-deformed Jaynes-Cummings model, we investigate the interaction between a two-level atom and a single-mode field, which is organized to be a MNCS. For this, the time evolution of population inversion and the nonclassical properties of the field, including the Mandel q-parameter, normal squeezing, and amplitude-squared squeezing, across various parameters and values of M is studied. It is found that in the presence of the intensity-dependent coupling and Kerr medium in the resonance condition, the nonclassical feature of squeezing occurs periodically during the interaction. Furthermore, sub-Poissonian photon statistics is also evident as a significant nonclassical feature. Finally, by measuring the field entropy for all the investigated cases, we examine the entanglement dynamics and determine the degree of atom-field entanglement. Additionally, a general comparison between the interaction of a two-level atom with the Mth coherent states (MCSs) and the interaction of a two-level atom with the MNCSs is presented.

KEYWORDS: F-Deformed Jaynes–Cummings, Model Mth nonlinear coherent states, Nonclassical properties, Quantum entanglement.

I. INTRODUCTION

The Jaynes-Cummings model (JCM) [1] is recognized as one of the most effective and comprehensive models in quantum optics. This model demonstrates the quantum behavior of the interaction between a two-level atom within a cavity and a single-mode electromagnetic field. Because of its importance in quantum optics and lasers, the JCM model has been extensively examined theoretically and experimentally by numerous authors over the past 50 years [2]-[4]. The time evolution of the system has been realized to be significantly dependent on the initial electromagnetic field statistical features. For example, it was found that if the initial radiation field is the standard coherent state (CS), quantum theory anticipates the collapses and revivals phenomenon for atomic inversion [5]-[7]. In addition, it was found that the JCM also shows the dynamics of the other quantum phenomena, such as the anti-bunching effect, field squeezing, and atom-field entanglement [8]-[10].

Because the JCM has been considered the standard model in quantum optics, the generalization of this model has been of interest to researchers in various ways, and many articles have extended this model using various methods. For example, the Tavis-Cummings model [11] is the generalization of the JCM that takes into account the interaction between a set of two-level atoms and a field. Furthermore,

there have been many models that investigate the field evolution in the existence of a Kerr-like medium by combining nonlinear parameters in terms of the photon number operator [12]-[14]. In addition, other extensions modify the dynamics equations, including the use of a two-level atom moving through an optical cavity length [15], [16], the fractional Schrodinger equation [17], [18], and a time-dependent field [19]. Also, previous studies have explored the quantum properties of the interaction between multi-level atoms and a single-mode electromagnetic field within a Kerr-like medium with an intensity-dependent coupling [20]-[25].

On the other hand, the standard JCM employs various fields or quantum states to explore atom-field interactions. One of these states is the Fock state, also known as the number state [7]. It was found that when the initial field is in a Fock state, the system displays Rabi oscillations in the atomic inversion, which represents the periodic exchange of energy between the atom and the field. The coherent state (CS) is another quantum state widely used in the JCM and its extensions [26]. Applying the CSs shows many patterns of revival and collapse phenomena that depend on the average number of photons. Among the other field modes applied to the standard JCM, we can refer to the generalizations of the standard CSs. One of these generalizations is called nonlinear coherent states (NCSs) [27]. These kinds of states were extended by Manko et al. by using the concept of a generalized f-oscillator [28]. They performed this extension by using the definition of the generalized annihilation operator, denoted as $\hat{A} = \hat{a}f(\hat{n})$, where $f(\hat{n})$ represents an operator-valued nonlinearity function in terms of the number operator $\hat{n} = \hat{a}^{\dagger}\hat{a}$ [28], [29]. Studies have shown that the NCSs, which are specifically characterized as the eigenstates of $\hat{A}$, have remarkably nonclassical features versus the normal CSs [30]- [32]. Also, it has been shown that the "superposition of the nonlinear coherent states" generated by expanding the standard superposed states have specific nonclassical features, which are absent in their particular

components [33]-[35]. Furthermore, by using the notion of the f-oscillator, a specific type of nonlinear JCM (NJCM) has been introduced known as f-deformed JCM, as the generalization of the standard JCM. This generalization demonstrates the interaction between a single mode of the electromagnetic field with a two-level atom in the presence of a nonlinear Kerr-like medium [36]. The primary benefit of this model is that, by considering the medium with a f-deformed oscillator rather than a regular harmonic oscillator, it is possible to analyze the development and interaction of NCSs with a two-level atom. The quantum properties of the interaction of a superposition of the NCSs with a two-level atom in a Kerr-like medium with intensity-dependent coupling have been studied [37]. Moreover, this interaction system has been potentially considered as an approach to produce a special kind of nonclassical states [38].

In recent years, a new state known as the "near coherent state" has been introduced and extended [39]- [41]. These states represent the particular superposition of two nearly equal CSs. Lately, based on the concept of the near-CSs, Othman A proposed a new state named the Mth coherent state (MCS) [42]. These states are called the MCSs because they are achieved by applying M times the number operator to the CSs. The MCSs exhibit important nonclassical features, such as sub-Poissonian statistics and squeezing, especially when they have a high mean photon number. In the other paper, the interaction between a single-mode electromagnetic field with a two-level atom in a Kerr-like medium and intensity-dependent coupling has been studied by assuming the initial field as the MCSs [43]. Recently, we have introduced new states using the concepts of the NCSs and the MCSs. These states, which are termed as Mth nonlinear coherent states (MNCSs), are obtained by applying M times the number operator to the NCSs [44]. They can also be considered as the result of adding and removing photons M times from a nonlinear coherent state. It was found that these states have significant nonclassical features such as sub-Poissonian photon statistics and amplitude squeezing. Therefore, investigating the

interaction of such states with a two-level atom and multi-level atoms can be interesting from a physical perspective.

The main point of this article is to study the interaction between a two-level atom within a lossless cavity and a single-mode electromagnetic field. This investigation is done in the presence of intensity-dependent coupling and a nonlinear Kerr medium. While dissipation is important in our problem, to gain the properties of the system, we first analyze the ideal situation in which no dissipation occurs. For this purpose, in section II, we describe this interaction system in the framework of the f-deformed JCM, where the initial radiation field is prepared to be the MNCSs. In section III, we study the atomic inversion temporal evolution of the interaction system for different cases. Next, in section IV, we analyze the dynamics of the field among the interaction by investigating the nonclassical properties like sub-Poissonian statistics, normal squeezing, and amplitude-squared squeezing of the radiation field. As an important feature of the quantum systems, the atom-field entanglement has been perused in section V by considering the time evolution of the field entropy. Finally, the discussion and results are presented in section VI.

II. INTERACTION BETWEEN A TWO-LEVEL ATOM AND AN MTH NONLINEAR COHERENT STATE

We begin by presenting the standard JCM [1], which is acknowledged as one of the most fundamental and analytical atom-field interaction models in quantum optics. It provides a clear and insightful framework for understanding the interaction between a single-mode electromagnetic field and a two-level atom within an ideal and lossless cavity. The Hamiltonian governing this interaction, derived under the rotating wave approximation and within the dipole approximation, is expressed as ($\hbar = c = 1$):

$$\hat{H}_{JC} = \hbar \upsilon \hat{a}^\dagger \hat{a} + \frac{1}{2}\hbar \omega \hat{\sigma}_z + \hbar \lambda \left(\hat{\sigma}_+ \hat{a} + \hat{a}^\dagger \hat{\sigma}_- \right). \quad (1)$$

In this equation, the first two phrases correspond to the operators of energy of the free electromagnetic field and the two-level atom when no interaction is present. On the other hand, the third term represents the interaction between atom-field, describing the dynamics of the energy exchange between the field and the atom. Additionally, ω represents frequency of the atomic transition, υ denotes the field frequency, the operators $\hat{a}$ and $\hat{a}^\dagger$ are responsible for creating and annihilating photons with the commutation relation $[\hat{a}, \hat{a}^\dagger] = 1$ and λ shows the coupling constant. Please note that the atomic operators are $\hat{\sigma}_z = |e\rangle\langle e| - |g\rangle\langle g|$, $\hat{\sigma}_+ = |e\rangle\langle g|$ and $\hat{\sigma}_- = |g\rangle\langle e|$ with $[\hat{\sigma}_z, \hat{\sigma}_\pm] = \pm 2\hat{\sigma}_\pm$ and $[\hat{\sigma}_+, \hat{\sigma}_-] = \hat{\sigma}_z$. We assume that $|e\rangle$ and $|g\rangle$, respectively, are the atom excited and ground states. On the other hand, the f-deformed JCM Hamiltonian is expressed as follows by using the generalized annihilation and creation operators:

$$\hat{H}_{NJC} = \hbar \upsilon \hat{A}^\dagger \hat{A} + \frac{1}{2}\hbar \omega \hat{\sigma}_z + \hbar \lambda \left(\hat{\sigma}_+ \hat{A} + \hat{A}^\dagger \hat{\sigma}_- \right), \quad (2)$$

where the operators $\hat{a}$ and $\hat{a}^\dagger$ in Eq. (1) have been substituted with the generalized operators $\hat{A}$ and $\hat{A}^\dagger$ defined as [28]:

$$\hat{A} = \hat{a}f(\hat{n}) = f(\hat{n}+1)\hat{a}$$
$$\hat{A}^\dagger = f(\hat{n})\hat{a}^\dagger = \hat{a}^\dagger f(\hat{n}+1), \quad (3)$$

with:

$$\left[\hat{A}^\dagger, \hat{A} \right] = (\hat{n}+1)f^2(\hat{n}+1) - \hat{n}f^2(\hat{n}). \quad (4)$$

It is worth mentioning that Eq. (2) consists of three terms: the first one represents the transformed free field Hamiltonian, the second one represents the atom energy operator, and the last term represents the atom-field interaction [45], [46]. The atom-field coupling in the interaction part of the Hamiltonian becomes intensity-dependent due to the nonlinearity of the function $f(\hat{n})$. Here, $f(\hat{n})$ is assumed to be a real function. The principal

distinction between Eq. (1) and Eq. (2), which represent different physical structures, are found in the nonlinearity of the deformed function $f(\hat{n})$. This indicates that the choice of $f(\hat{n})$ can significantly change the physical characteristics of the system, potentially resulting in unique nonlinear behaviors in the atom-field interaction. In this study we use the following nonlinearity function to obtain specific physical results [31], [37]:

$$f(\hat{n}) = \sqrt{1 - \frac{\chi}{\upsilon}\left(1 - \hat{n}^{k-1}\right)}. \qquad (5)$$

In this equation, χ shows the dispersive part of the third-order nonlinearity of the Kerr medium ($0 \leq \chi << \upsilon$) and $k \geq 1$. It is worth noting that, applying $f(\hat{n})$ demonstrated in Eq. (5) with $k = 2$ as a specific instance, the NJCM (Eq. (2)) can be utilized to describe a system in which a two-level atom surrounded by a Kerr medium. Meanwhile, the properties of the applied field are modified, because of a nonlinear intensity-dependent coupling between the atom and the field that results from the existence of the medium [47].

There are different approaches to solving the f-deformed JCM. For example, the time-dependent Schrödinger equation method and the density operator approach have been presented in [36] and [37] respectively. In the interaction picture, the Hamiltonian in Eq. (2) becomes:

$$\hat{H}_I = \hbar\lambda\left[\hat{\sigma}_+ e^{i\Omega_{\hat{n}}t}\hat{A} + \hat{A}^\dagger e^{-i\Omega_{\hat{n}}t}\hat{\sigma}_-\right], \qquad (6)$$

where $\Omega_{\hat{n}} = \omega - \upsilon\left[\hat{A}, \hat{A}^\dagger\right]$ is a generalized detuning.

The wave function $|\psi\rangle$ at each time t is expressed as an expansion in terms of the states $|e, n\rangle$, and $|g, n+1\rangle$ as below:

$$|\psi(t)\rangle = \sum_{n=0}^{\infty} q_n\left(A_{n+1}(t)|g, n+1\rangle + B_n(t)|e, n\rangle\right), \qquad (7)$$

in which the values A and B represent the probability amplitudes and q_n denotes the amplitude of the state $|n\rangle$. The probability amplitudes $A_{n+1}(t)$ and $B_n(t)$ are obtained as follows by solving the Schrödinger equation within the interaction:

$$A_{n+1}(t) = \frac{-2i\lambda\sqrt{n+1}f(n+1)}{\Phi_n}\sin\left(\frac{\Phi_n t}{2}\right)e^{-\frac{i\Omega_n t}{2}}, \qquad (8)$$

$$B_n(t) = \left[\cos\left(\frac{\Phi_n t}{2}\right) - \frac{i\Omega_n}{\Phi_n}\sin\left(\frac{\Phi_n t}{2}\right)\right]e^{\frac{i\Omega_n t}{2}}. \qquad (9)$$

In these equations, $\Phi_n = \sqrt{\Omega_n^2 + 4\lambda(n+1)f^2(n+1)}$ represents a generalized Rabi frequency. To obtain the specific physical properties of interest, we must only determine the distribution of the initial field photon number $|q_n|^2$. We considered the Mth nonlinear coherent state (MNCSs) as the applied field in this interaction model in the following. These states are defined by applying the number operator M times to the NCSs as below [44]:

$$|M(\alpha, f)\rangle = N_M^f \sum_{n=0}^{\infty} \frac{n^M \alpha^n}{[f(n)!]\sqrt{n!}}|n\rangle, \qquad (10)$$

where $f(n)! = f(1)f(2)f(3)...$ and $f(0)! = 1$ [28], [34]. In addition, the normalization coefficient N_M^f is determined from the normalization condition as follows [44]:

$$N_M^f = \left(\sum_{n=0}^{\infty} \frac{n^{2M}|\alpha|^{2n}}{[f(n)!]^2 n!}\right)^{-1/2}. \qquad (11)$$

Based on the concept of the MNCSs, when *M*=0 and $f(\hat{n}) = 1$, the coherent states are obtained and by choosing *M*=0 when we have $f(\hat{n})$, the NCSs are gained. Furthermore, for $f(\hat{n}) = 1$ and different *M* values, the MCSs are derived.

Using Eq. (10), the mean number of the photons is:

$$\langle \hat{n} \rangle_M = \left| N_M^f \right|^2 \sum_{n=0}^{\infty} \frac{n^{2M+1} |\alpha|^{2n}}{\left[f(n)! \right]^2 n!}. \tag{12}$$

For a specific value of α, it has been observed that the MNCSs photon distribution function is the same as a Poissonian distribution but with a shift that depends on M. To ensure that all the photonic distributions of the various MNCSs have an identical position, they should be centered at one position. This alignment is achieved using the computational methods outlined in [44]. As we mentioned in the definition of the MNCSs, we replace the parameter of α with α_P^M, which is defined as follows:

$$\alpha_P^M = \exp \left\{ \frac{1}{2} \left[\psi \left(|\alpha|^2 + 1 \right) + \right. \right. \tag{13}$$
$$\left. \left. \psi \left(f \left(|\alpha|^2 \right) f' \left(|\alpha|^2 \right) + 1 \right) \right] - \frac{M}{|\alpha|^2} \right\} e^{i\theta}.$$

where $f \left(|\alpha|^2 \right)$ represents the deformed function, $f' \left(|\alpha|^2 \right)$ denotes the first derivative of the deformed function, θ displays the coherent parameter phase, and $\psi(x) = \Gamma'(x) / \Gamma(x)$ is the digamma function. It was found that for a given α, the NCSs and the MNCSs produce nearly an equal mean number of photons. To understand this clearly, please look at Table 1, which shows that the various amounts of M for the same α have approximately identical mean photon numbers, but the α_P^M values have significant differences.

In this study, to investigate the interaction between a two-level atom and an MNCS, we generally use $M = 0, 1, 10, 50,$ and 100, as given in Table 1. We will initially consider the field to be an MNCS, where the amplitude of the applied field is obtained as follows:

$$q_n = \left[\sum_{n=0}^{\infty} \frac{n^{2M} \left| \alpha_p^M \right|^{2n}}{n! \left[f(n)! \right]^2} \right]^{-\frac{1}{2}} \left[\frac{n^M \left(\alpha_p^M \right)^n}{\sqrt{n!} \left[f(n)! \right]} \right]. \tag{14}$$

In addition, in all numerical and analytical computations, we consider that the amounts of Ω_n, Φ_n, and χ are scaled with the coupling constant λ [37], [43].

Table 1. The table shows the selected values of M with a steady $I\alpha$. We observe that the mean number of photons from Eq. (12) is almost conserved, and the value of α_p^M from Eq. (13) with parameters $\chi = 0.4\lambda$, $\lambda = 0.003$, $\nu = 1$, and $k=2$ has a significant variation.

M	α	α_p^M	$\langle \hat{n} \rangle$
0	5	5.05637	24.827
1	5	4.85811	24.876
10	5	3.38939	25.0286
50	5	0.684305	25.0466
100	5	0.0926107	25.0311

III. EVOLUTION OF ATOMIC INVERSION

The atomic inversion which is the difference in probability between an excited state of the atom and its ground state plays a significant role in atom-field interactions. It has been found that atomic inversion is particularly sensitive to the statistical characteristics of the applied field. If the primary electromagnetic field is in a CS, the collapse and revival phenomena will occur as completely quantum mechanical properties, as previously confirmed by experimental observation [6]. Investigating the collapse and the revival duration of fluctuations in the atomic inversion is a simple technique to gain useful knowledge of the atom-field interaction systems. By considering Eq. (7), the atomic inversion would be obtained as follows:

$$W(t) = \sum_{n=0}^{\infty} |q_n|^2 \left(\left| B_n(t) \right|^2 - \left| A_{n+1}(t) \right|^2 \right). \tag{15}$$

Inserting Eq. (8) and Eq. (9) in Eq. (15) with $k = 2$ and $\nu = 1$, would result in:

$$W(t) = \sum_{n=0}^{\infty} |q_n|^2 \left[\frac{\Omega_n^2}{\Phi_n^2} + \frac{4\lambda^2 (n+1)(1+\chi n)}{\Phi_n^2} \cos(\Phi_n t) \right], \tag{16}$$

where $\Omega_n = \Delta - 2\chi n$, and $\Delta = \omega - \upsilon$ is the atom-field detuning.

The time evolution of Eq. (16), in terms of the scaled time $\tau = \lambda t$ for the applied field defined in Eq. (14), is plotted in Fig. 1. For various parameters and different values of *M*, we notice that the behavior of the population inversion of our system with an MNCS field is similar to that of a system with a general NCS field. We can observe that the position of the peaks is essentially preserved. As displayed in Figs. 1d, e, and f, the closest and most similar case to the CSs (Fig. 1a) and the NCSs (Figs. 1b and c) is for *M*=1 (blue curves), and we named this case as first NCS. According to these figures, we can hardly notice the differences between the MNCSs and the NCSs. Meanwhile, these differences become more apparent as the value of *M* increases, for example, when *M*=50 and *M*=100.

The first column of Fig. 1 indicates the linear state (the MCSs) when $\chi = 0$ and $\Delta = 0$. We can see that the discrete packet positions are almost identical. These packets show the phenomenon of atomic revival and collapse [48], [49]. Recall that the collapse, which represents the destructive interference between the probability amplitudes, occurs when the fluctuation packets reach zero. Also, constructive interference happens during times of revival. Furthermore, we observe that as the value of *M* increases, the number of revivals and collapses increases (see Figs. 1(j) and (m)).

In the middle and last column of Fig. 1, we have shown the atomic inversion temporal evolution in the presence of the nonlinear Kerr medium with set values of *M* for resonance ($\Delta = 0$) and nonresonance ($\Delta \neq 0$) cases. We observe that fluctuations of the atomic inversion are more periodic in the resonance case than in the nonresonance case. The structure of these fluctuations in the case of resonance is also completely different from the linear state. The main reason for this difference is the effect of the parameter χ on the generalized Rabi frequency in the f-deformed JCM. In addition, for the case $\Delta = 0$, we can see that raising the

value of *M* increases the revival time (see Figs. 1(k) and 1(n)). Moreover, compared to the MCSs, the MNCSs in the resonance condition are usually more periodic. This is even though for the case $\Delta \neq 0$, the growth in *M* enhances the collapse time, which means that the collapses and revivals become more obvious (see Fig. 1l and Fig. 1o). Also, raising *M* leads to an expansion in the fluctuation range and the number of revivals and collapses, while for $\Delta = 0$, the range and the number of packets are almost constant.

IV. THE DYNAMICS OF FIELD

A. *Statistical features of the field*

The study of Mandel *q*-parameter [50] is an extremely efficient method for describing the statistical characteristics of a state. This parameter defines the photon distribution normalized variance and is determined as below:

$$q = \frac{\left\langle \left(\Delta \hat{n}\right)^2 \right\rangle - \left\langle \hat{n} \right\rangle}{\left\langle \hat{n} \right\rangle}, \qquad (17)$$

where $\left\langle \left(\Delta \hat{n}\right)^2 \right\rangle = \left\langle \hat{n}^2 \right\rangle - \left\langle \hat{n} \right\rangle^2$. It is important to note that, based on the amount of the Mandel *q*-parameter, the field could have Poissonian statistics when *q*=0 super-Poissonian statistics when *q*>0 and sub-Poissonian statistics when *q*<0. In addition, the field is nonclassical if it has sub-Poissonian photon statistics [51]. Using the wave function of Eq. (7), we can easily obtain the expected values as follows:

$$\left\langle \hat{n} \right\rangle = \sum_{n=0}^{\infty} \left| q_n \right|^2 \left[n + \left(1 - \frac{\Omega_n^2}{\Phi_n^2} \right) \sin^2 \left(\frac{\Phi_n t}{2} \right) \right], \quad (18)$$

And

$$\left\langle \hat{n}^2 \right\rangle = \sum_{n=0}^{\infty} \left| q_n \right|^2 \left[n^2 + \left(2n + 1 \right) \right.$$
$$\left. \left(1 - \frac{\Omega_n^2}{\Phi_n^2} \right) \sin^2 \left(\frac{\Phi_n t}{2} \right) \right]. \qquad (19)$$
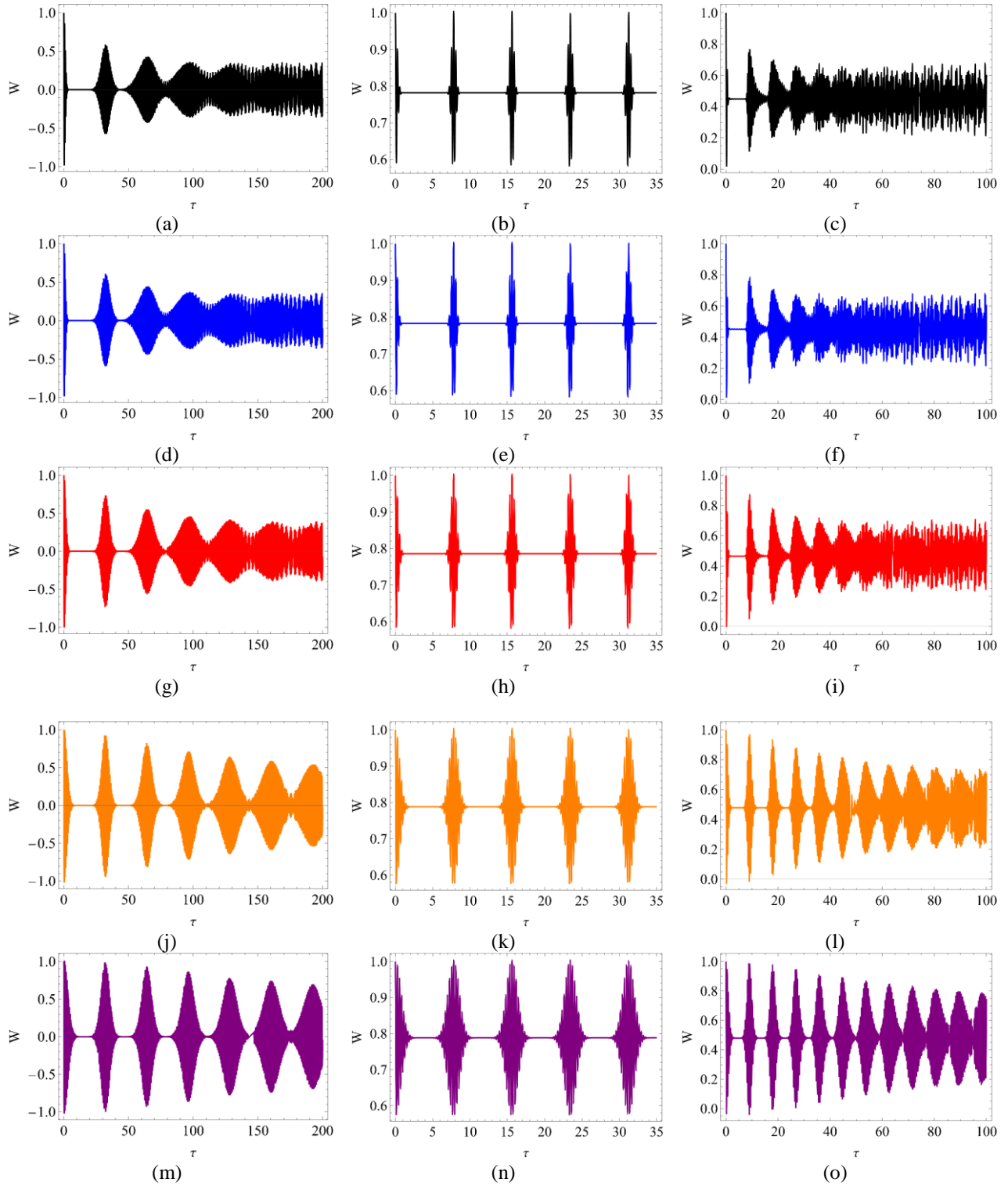
Fig. 1. The evolution of the atomic inversion $W(t)$ against scaled time τ. The y-axis represents the atomic inversion, and the x-axis shows the scaled time $\tau = \lambda t$. The black curves are for $M=0$, the blue curves are for $M=1$, the red curves are for $M=10$, the orange curves are for $M=50$, and the purple curves are for $M=100$. The first column from the left is for the linear state (the MCSs) with $\chi = \Delta = 0$. The middle column is for the nonlinear states (the MNCSs) with $\chi = 0.4\lambda$, $\lambda = 0.003$ and $\Delta = 0$. Finally, the last column is for the nonlinear states (the MNCSs) with $\chi = 0.4\lambda$, $\lambda = 0.003$, and $\Delta = 0.03$. All figures are with $|\alpha| = 5$.

The q-parameter as a function of the scaled time τ is displayed in Fig. 2. We can observe the q-parameter behavior for each of our chosen M values in the first row. Please note

that the first row is the magnified image that displays all the MNCSs, while the second row is given as an example to show more details of one specific MNCS. At first glance, we can see that the q-parameter is negative for all the investigated values. This implies that the cavity field photon statistics are sub-Poissonian throughout the entire interaction period, which indicates a significant nonclassical feature of the interaction system. Also, we observe that even though each column has distinct χ and Δ values, the q-parameter for every given value of M

somehow oscillates close to its main amount. In other words, for a specific M, the center of the oscillations is approximately stable for various physical parameters. The first column is related to the condition of $\chi = 0$, and $\Delta = 0$ ($f(n) = 1$). We can see that in this case, by increasing the value of M, the place of the fluctuations is nearly conserved, while the width and the height of the fluctuations reduce. Furthermore, it is clear that, as M rises, the value of the q-parameter becomes more negative and the distribution of the photon statistics becomes fully sub-Poissonian.
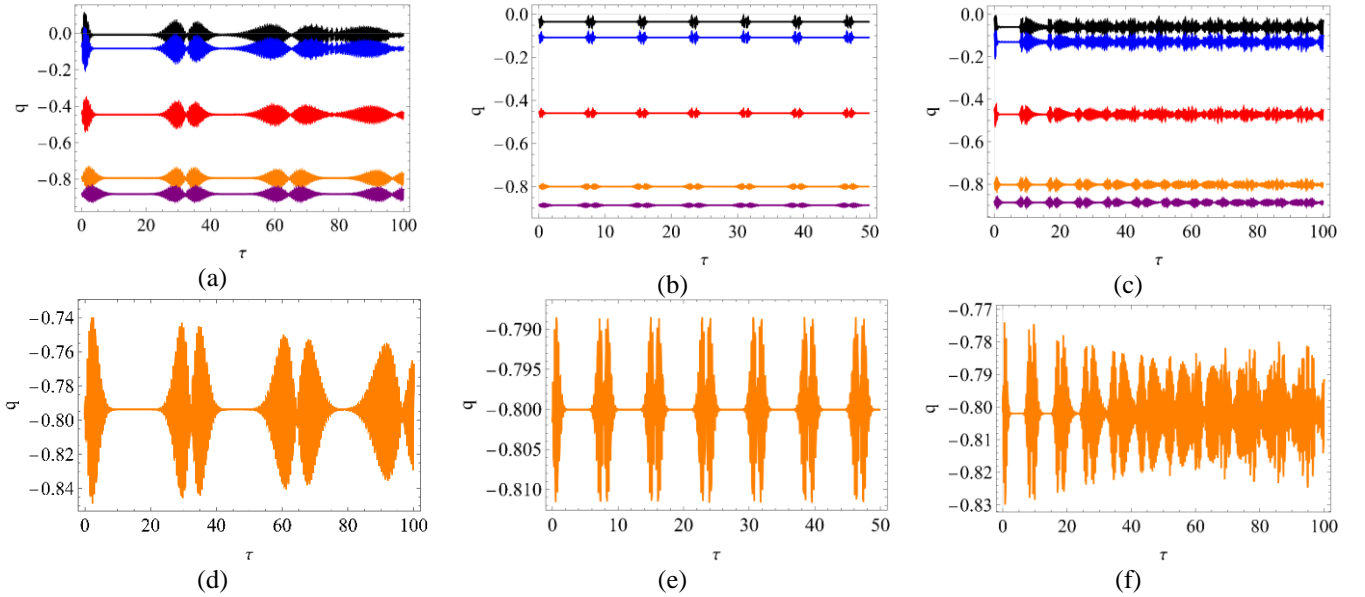

Fig. 2. The temporal evolution of the q-parameter against the scaled time. The y-axis represents the q-parameter, and the x-axis shows the scaled time $\tau = \lambda t$. The black curves are for M=0, the blue curves are for M=1, the red curves are for M=10, the orange curves are for M=50, and the purple curves are for M=100. The first column from the left is for the linear case (the MCSs) with $\chi = \Delta = 0$. The middle column is for the nonlinear case (the MNCSs) with $\chi = 0.4\lambda$, $\lambda = 0.003$ and $\Delta = 0$. Finally, the last column is for the nonlinear states (the MNCSs) with $\chi = 0.4\lambda$, $\lambda = 0.003$, and $\Delta = 0.03$. All figures are with $|\alpha| = 5$. The first row is for all the studied Ms. The second row is for the case when M=50 with more detail from the first row.

The middle column in Fig. 2 is plotted for the case where the primary field is nonlinear (the MNCSs) with $\chi = 0.4\lambda$ and $\Delta = 0$. We notice that as M grows, the q-parameter becomes more negative, similar to the pattern in the first column. In addition, it is clear that the increase of M leads to more decreases in the height and width of the packets than in the case of $f(n) = 1$, while the oscillations become more periodic. Also, we can see that the position of the fluctuations is relatively preserved. Finally,

in the last column, we have plotted the q-parameter for the initial field of the interaction system in the nonresonance situation with the values $\chi = 0.4\lambda$ and $\Delta = 0.03$. We observe that, over time of the interaction, as the value of M grows, the number of fluctuations increases while their height reduces. In general, we can observe that the fluctuations are more periodic in the resonance case compared to the nonresonance case. However, like in the previous cases in the

nonresonance mode as the *M* value grows, the *q*-parameter becomes more negative, and the photon statistic is completely sub-Poissonian.

B. *Normal Squeezing*

The amplitude squeezing of the field is one of the important nonclassical features that we have investigated in this section. Reduced fluctuations in one of the momentum or position quadratures of the field exchanged with increased fluctuations in the other describe a squeezed state [7]. To obtain normal squeezing, consider the Hermitian operators as below:

$$\hat{X}_1 = \frac{1}{2}\left(\hat{a} + \hat{a}^\dagger\right) \text{ and } \hat{Y}_1 = \frac{1}{2i}\left(\hat{a} - \hat{a}^\dagger\right). \qquad (20)$$

The uncertainty for the amplitude and phase quadratures by the commutation relation $\left[\hat{X}_1, \hat{Y}_1\right] = i / 2$ is:

$$\left\langle\left(\Delta\hat{X}_1\right)^2\right\rangle\left\langle\left(\Delta\hat{Y}_1\right)^2\right\rangle \geq 1/16. \qquad (21)$$

where, $\Delta\hat{X}_1$ and $\Delta\hat{Y}_1$ respectively are uncertainties in the quadratures of $\hat{X}_1$ and $\hat{Y}_1$. Please notice that the normal squeezing occurs when one of the inequalities $\left(\Delta\hat{X}\right)^2 < 1/4$ or $\left(\Delta\hat{Y}\right)^2 < 1/4$, is satisfied. Under these conditions, normal squeezing parameters have been determined for each of the operators as follows [52]:

$$S_X^{(1)} = 4\left\langle\left(\Delta\hat{X}_1\right)^2\right\rangle - 1 \ \& \ S_Y^{(1)} = 4\left\langle\left(\Delta\hat{Y}_1\right)^2\right\rangle - 1. \qquad (22)$$

It is well known that when the value of the squeezing parameter in $\hat{X}_1$ or $\hat{Y}_1$ is negative, a quantum state is squeezed. Thus, using the annihilation and creation operators of the photon, the normal squeezing parameters can be obtained using the following inequality equations:

$$S_X^{(1)} = \left\langle\hat{a}^2\right\rangle + \left\langle\hat{a}^{\dagger 2}\right\rangle + 2\left\langle\hat{n}\right\rangle - \left(\left\langle\hat{a}\right\rangle + \left\langle\hat{a}^\dagger\right\rangle\right)^2 < 0, \qquad (23)$$

$$S_Y^{(1)} = 2\left\langle\hat{n}\right\rangle - \left\langle\hat{a}^2\right\rangle - \left\langle\hat{a}^{\dagger 2}\right\rangle + \left(\left\langle\hat{a}\right\rangle - \left\langle\hat{a}^\dagger\right\rangle\right)^2 < 0. \qquad (24)$$

To determine the amount of the normal squeezing of the applied field, we calculate the expectation values in Eqs. (23) and (24) for the proposed system. We notice that Eq. (18) yields the expectation value for $\left\langle\hat{n}\right\rangle$, and $\left\langle\hat{a}^r\right\rangle$ is achieved as below: ($\left\langle\hat{a}^{\dagger r}\right\rangle = \left\langle\hat{a}^r\right\rangle^*$):
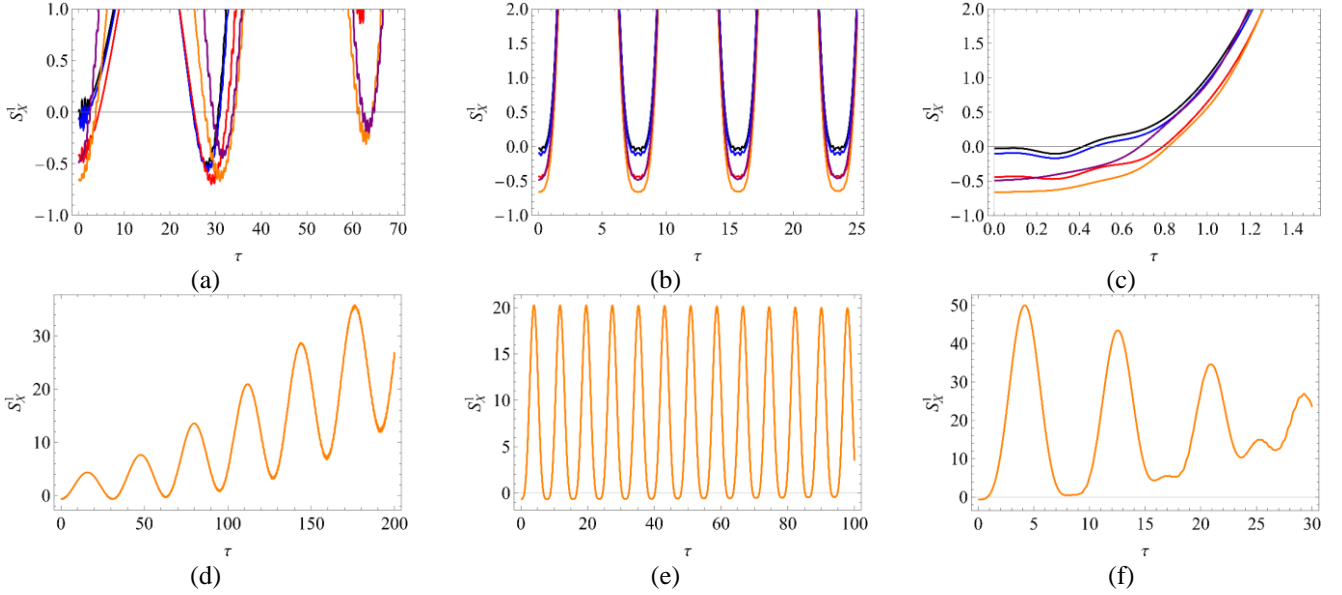
$$\left\langle\hat{a}^r\right\rangle = \sum_{n=0}^{\infty} q_n^* q_{n+r}\left[A_{n+1}^* A_{n+r+1}\sqrt{\frac{(n+r+1)!}{(n+1)!}} + B_n^* B_{n+r}\sqrt{\frac{(n+r)!}{(n)!}}\right]. \qquad (25)$$

Figure 3 displays the time evolution of the normal squeezing function $S_x^{(1)}$ for the values considered in Fig. 2. In Fig. 3(a), with $\chi = \Delta = 0$, it is clear that increasing the order of the initial field *M* leads to the normal squeezing in the quadrature $\hat{X}_1$ in the specific time intervals during the interaction time. It is while, as the interaction progresses, the squeezing gradually reduces and eventually disappears. In addition, while raising the order of the MNCSs to the value of *M*=50, the squeezing depth also increases, while for *M*=100, the squeezing depth is decreased.

The middle and last columns of Fig. 3 demonstrate the nonlinear case in the existence of the Kerr medium and intensity-dependent coupling. In the middle column, we have plotted the time evolution of $S_x^{(1)}$ when the atom-field interaction is resonant. It has been observed that the nonclassical feature of normal squeezing in the quadrature $\hat{X}_1$ occurs periodically at specific time intervals during the interaction time. These periodic fluctuations have a more regular and sinusoidal shape due to the presence of χ. The MNCSs are more squeezed than the MCSs, which is a significant characteristic of the studied interaction system. We can see that, as *M* is raised to a specific value, the depth of the valleys and degree of squeezing increase,

similar to the linear state shown in the first column. In the nonresonance case, as shown in the last column, we see that the normal squeezing in the quadrature $\hat{X}_1$ happens in a short period of time at the beginning of the

interaction. We also observe that similar to previous cases, the squeezing degree increases as M grows up to $M = 50$. Moreover, unlike the resonance case, the squeezing disappears over time.

Fig. 3. The same as in Fig. 2 but for the time evolution of the normal squeezing parameter $S_x^{(1)}$.

C. *Amplitude-squared squeezing*

In this section, we study amplitude-squared squeezing as another nonclassical feature in the atom-field interaction. To study this feature, the operators $\hat{X}_2$ and $\hat{Y}_2$, which are Hermitian defined as follows [53], [54]:

$$\hat{X}_2 = \frac{1}{2}\left(\hat{a}^2 + \hat{a}^{\dagger 2}\right) \text{ and } \hat{Y}_2 = \frac{1}{2i}\left(\hat{a}^2 - \hat{a}^{\dagger 2}\right), \quad (26)$$

with $\left[\hat{X}_2, \hat{Y}_2\right] = i\left(2\hat{n} + 1\right)$. In addition, Heisenberg uncertainty relation for the quadrature operators $\hat{X}_2$ and $\hat{Y}_2$ is specified as follows:

$$\left\langle\left(\Delta\hat{X}_2\right)^2\right\rangle\left\langle\left(\Delta\hat{Y}_2\right)^2\right\rangle \geq \frac{1}{4}\left|\left\langle i\left(2\hat{n}+1\right)\right\rangle\right|^2. \quad (27)$$

The studied case holds the property of amplitude-squared squeezing if either of the

circumstances $\left\langle\left(\Delta\hat{X}_2\right)^2\right\rangle < \left\langle\hat{n}+\frac{1}{2}\right\rangle$ or $\left\langle\left(\Delta\hat{Y}_2\right)^2\right\rangle < \left\langle\hat{n}+\frac{1}{2}\right\rangle$ is satisfied.

Now, by using the normalized parameters that are expressed as follows:

$$S_X^{(2)} = \frac{\left\langle\left(\Delta\hat{X}_2\right)^2\right\rangle}{\left|\left\langle\hat{n}+\frac{1}{2}\right\rangle\right|} - 1 \quad \&$$

$$S_Y^{(2)} = \frac{\left\langle\left(\Delta\hat{Y}_2\right)^2\right\rangle}{\left|\left\langle\hat{n}+\frac{1}{2}\right\rangle\right|} - 1,$$

$$(28)$$

and using Eq. (26) we have:

$$S_X^{(2)} =$$

$$\frac{\left\langle\hat{a}^4\right\rangle + \left\langle\hat{a}^{\dagger 4}\right\rangle + 2\left\langle\hat{n}^2\right\rangle - 2\left\langle\hat{n}\right\rangle - \left(\left\langle\hat{a}^2\right\rangle + \left\langle\hat{a}^{\dagger 2}\right\rangle\right)^2}{4\left\langle\hat{n}\right\rangle + 2}, \quad (29)$$

$$S_Y^{(2)} =$$

$$\frac{2\langle \hat{n}^2 \rangle - 2\langle \hat{n} \rangle - \langle \hat{a}^4 \rangle - \langle \hat{a}^{\dagger 4} \rangle + \left(\langle \hat{a}^2 \rangle - \langle \hat{a}^{\dagger 2} \rangle \right)^2}{4\langle \hat{n} \rangle + 2}. \quad (30)$$

Equations (18), (19) and (25) give the expectation values needed to determine the amplitude-squared squeezing of the studied system. Note that the state holds this feature if the value of parameters $S_X^{(2)}$ or $S_Y^{(2)}$ is less than 0.

Figure 4 shows the time evolution of $S_X^{(2)}$ for the same parameters and selected values as shown in Fig. 2. We can observe that the amplitude-squared squeezing happens in all the investigated cases as a nonclassical feature of the interaction system in the quadrature $\hat{X}_2$. In the linear case when $f(n) = 1$, this feature is seen in specific time intervals of interaction.

Also, in the nonlinear case when $\Delta = 0$ (Fig. 4(b)), we see that the oscillations are periodic

and the amplitude-squared squeezing occurs in certain time intervals of the interaction. Meanwhile, in the nonresonance case, when $\Delta = 0.03$, we see this nonclassical feature in a short duration at the beginning of the interaction. Also, we observed that in all these cases with the rise of M up to $M=10$, the degree of squeezing increases, and for the large value of M, the squeezing degree decreases. In addition, by comparing Figs. 4(b) and 3(b), it can be seen that the time interval of occurrence of amplitude-squared squeezing is very close to normal squeezing. However, the main difference between $S_X^{(2)}$ and $S_X^{(1)}$ is the frequency and period of the oscillations. In amplitude-squared squeezing, the frequency of the oscillations is almost twice that of normal squeezing, and the time of the period of the oscillations has nearly halved. Also, we can see that the maximum value of this nonclassical feature is when $M=10$, while this value occurs in the normal squeezing when $M=50$. Furthermore, we observe that when $M=100$, the squeezing feature is completely lost for the applied radiation field.
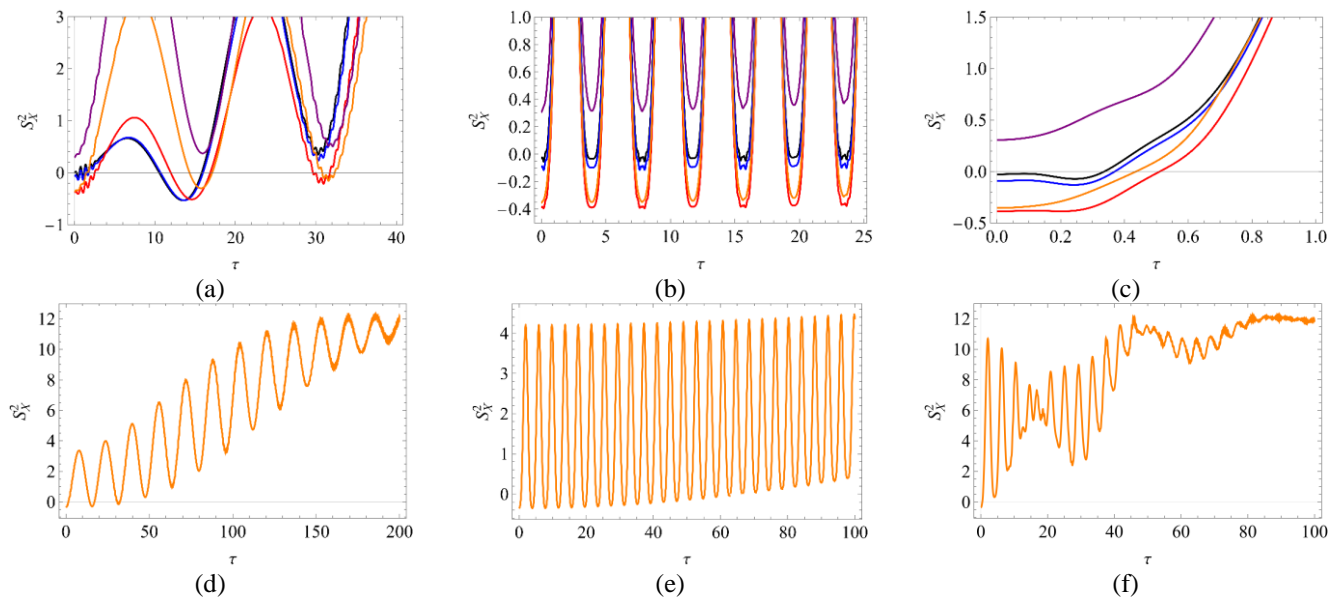

Fig. 4. The same as in Fig. 2 but for the time evolution of the amplitude-squared squeezing parameter $S_x^{(2)}$.

V. FIELD ENTROPY

Quantum entanglement is a fundamental characteristic of quantum systems, which acts as a basis for quantum computing and offers valuable applications in quantum information

science [55]-[57]. Within the framework of cavity quantum electrodynamics (QED), the interaction between atoms and fields offers a straightforward approach to generating quantum entangled states, that are essential for

the progress of quantum information processing systems [58]. There are many approaches to measuring entanglement. One of the typical methods to demonstrate the value of entanglement is the temporal evolution of the atom-field entropy [59]. It means that the higher the entropy implies the greater the amount of entanglement and inversely. One of the most effective methods for calculating entropy in quantum systems is using the Von Neumann reduced entropy, which measures the entropy of a system by focusing on its reduced density matrix [60]. The entropies of the field and the atom, as considered different systems, are determined using the Von Neumann entropy, defined as follows:

$$S_{A(F)}(t) = -Tr_{A(F)}\left(\hat{\rho}_{A(F)}(t)\ln\hat{\rho}_{A(F)}(t)\right), \quad (31)$$

where the subscript $A(F)$ represents the atom (field) and $\hat{\rho}_{A(F)}$ denotes the reduced density operator that for the atom is expressed as follows:

$$\hat{\rho}_A(t) = Tr_F(\hat{\rho}) = Tr_F(|\psi\rangle\langle\psi|). \quad (32)$$

In this study, $|\psi\rangle$ is given by Eq. (7), and the components of the density matrix are obtained as follows:

$$\begin{pmatrix} \rho_{11} & \rho_{12} \\ \rho_{21} & \rho_{22} \end{pmatrix} =$$

$$\begin{pmatrix} \sum_{n=0}^{\infty} q_n q_n^* |A_{n+1}|^2 & \sum_{n=0}^{\infty} q_n q_{n+1}^* A_{n+1} B_{n+1}^* \\ \sum_{n=0}^{\infty} q_n^* q_{n+1} A_{n+1}^* B_{n+1} & \sum_{n=0}^{\infty} q_n q_n^* |B_n|^2 \end{pmatrix}. \quad (33)$$

We know that for a pure state where $Tr(\hat{\rho}^2) = 1$, the entropy must be zero. In contrast, the entropy would no longer be zero for a mixed state, where $Tr(\hat{\rho}^2) < 1$. Taking into account the Araki and Lieb theorem [61] for quantum systems with two components, like the atom-field interaction system the triangle inequality limits the entropies as follows:

$$\left|S_A(t) - S_F(t)\right| \le S(t) \le \left|S_A(t) + S_F(t)\right|. \quad (34)$$

where $S(t)$ represents the general entropy of the combined atom and the field system at any time t. As the atom-field system at first is assumed to be within a pure state, it follows that for any time $t>0$, the atom and the field reduced entropies are equal, i.e., $S_A(t) = S_F(t)$. Hence, the focus can be placed on the evolution of the field entropy rather than the entropy of the atom.

Phoenix and Knight demonstrated that the reduced entropy of the Von Neumann could be described in terms of the eigenvalues of the reduced density matrix [10]. Thus, by applying Eq. (32), the entropy is expressed as follows:

$$S_F = S_A = -\left(\zeta_1 \ln \zeta_1 + \zeta_2 \ln \zeta_2\right), \quad (35)$$

in which ζ_1 and ζ_2 represent the eigenvalues of $\hat{\rho}_A$, which are determined as follows:

$$\zeta_1 = \frac{1}{2}\left[\rho_{11} + \rho_{22} + \sqrt{(\rho_{22} - \rho_{11})^2 + 4\rho_{12}\rho_{21}}\right], \quad (36)$$

and

$$\zeta_2 = \frac{1}{2}\left[\rho_{11} + \rho_{22} - \sqrt{(\rho_{22} - \rho_{11})^2 + 4\rho_{12}\rho_{21}}\right]. \quad (37)$$

Figure 5 illustrates the numerical results for the time evolution of the Von Neumann reduced entropy when the initial state of the cavity field is an MNCS. The plots in the first row present an overview of the curves for all values of *M*, including those shown in the bottom rows along with other MNCSs. The second row focuses on the case *M*=0, while the third row details the situation *M*=50. As mentioned in the previous sections, the first column from the left displays the entropy for the linear case when $\chi = 0$ and $\Delta = 0$. The middle column and the last column illustrate the temporal evolution of the field reduced entropy for $\chi = 0.4\lambda$, and display the resonance and nonresonance cases, respectively.
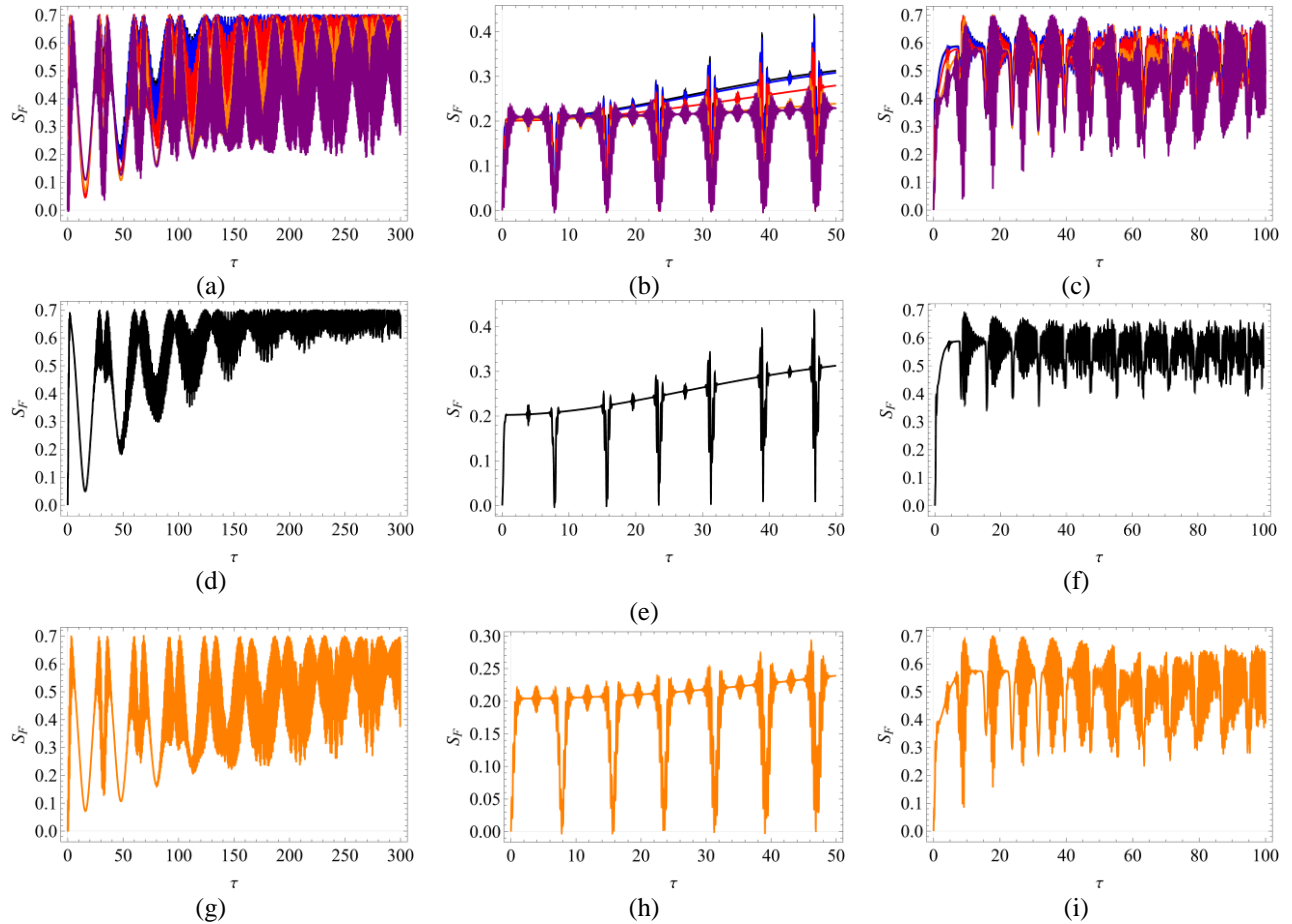
Fig. 5. The temporal evolution of the field entropy against the scaled time $\tau = \lambda t$. The black curves are for the NCSs or $M=0$, the blue curves are for $M=1$, the red curves are for $M=10$, the orange curves are for $M=50$, and the purple curves are for $M=100$. The first column from the left is for the linear case (the MCSs) with $\chi = \Delta = 0$. The middle column is for the nonlinear case (the MNCSs) with $\chi = 0.4\lambda$, $\lambda = 0.003$ and $\Delta = 0$. Finally, the last column is for the nonlinear case (the MNCSs) with $\chi = 0.4\lambda$, $\lambda = 0.003$ and $\Delta = 0.03$. All figures are with $|\alpha| = 5$. The first row is for all the studied Ms. The second and third rows are for the cases when $M=0$ and $M=50$, respectively, with more detail from the first row.

It is clear that in the absence of the intensity-dependent coupling and Kerr nonlinearity, the time evolution of the field reduced entropy shows a chaotic behavior (Fig. 5a). On the other hand, when $M=0$, we observe that the fluctuations decrease over time, and S_F approaches the semi-stable value more rapidly. However, the chaotic behavior increases with the rise of M. Hence, other M amounts need more time to achieve a slightly lower semi-stable value. In the nonlinear system under the resonance condition, shown in the middle column, the entropy behavior is completely different from the linear system. In this case, the evolution of the S_F exhibits a nearly regular behavior over the interaction time. Also, in this case, the collapse and revival

patterns occur as a nonclassical feature. Moreover, it is observed that similar to the linear case, growing the amount of M results in a reduced degree of atom-field entanglement. Also, the entropy of the field, or its equivalent, the degree of entanglement, is reduced in the presence of nonlinearity. In addition, it is notable that the entropy of the field becomes zero at specific times of the interaction, which indicates the disappearance of the entanglement. Notably, when the value of the entropy nears zero, the atom resides in either its lower or upper state, indicating a pure state. Moreover, as it is clear from the figures of the last column, in the nonlinear system in nonresonant conditions, there is a chaotic exhibit in the field entropy approximately the

same as in the linear case. We can see that in this case, the degree of the field entropy of the interaction system is greater than that of the nonlinear system when $\Delta = 0$, and as a result, the atom-field entanglement is greater. However, in this condition similarly to the previous cases as the order of the applied field increases, the amount of the field entropy reduces.

It is notable that, the purity of the field throughout the interaction is intrinsically linked to its quantum statistical properties [62]. In reality, when the field displays sub-Poissonian features, the field, and the atom can experience a reversible process, returning to their initial pure states at particular intervals during the interaction. In general, the behavior of the field entropy within this interaction system can be thoroughly described by considering the plots presented in Figs. 5 and 2. According to Fig. 2, we can see that in all the studied cases for the MNCSs with a rising value of M, the photon distribution of the field is completely sub-Poissonian. As a result, the field may approach the pure state almost during the atomic inversion revival times, which means that the degree of the entropy and equivalently, the amount of the entanglement will decrease or become zero.

VI. CONCLUSION

One of the most significant theoretical achievements in quantum optics is the development of a model that can determine the nonclassical features of interactions between atoms and fields. In this article, we study the interaction between a single two-level atom with a new class of nonlinear coherent state which we have introduced in [44] in the existence of an intensity-dependent coupling and a Kerr medium. For this purpose, we use the f-deformed Jaynes-Cummings model (JCM). In this framework, by selecting a suitable form of $f(n)$ in Eq. (5) with the specific amount of $k=2$, the nonlinearity for both the applied field and the atom-field intensity-dependent coupling has been guaranteed. In addition, the effects of the field order (M) on the dynamics of interaction have been examined.

Regarding the interaction system with a two-level atom, the first NCS (M=1) holds a unique position among all MNCSs. Because for all physical parameters examined, the first NCS demonstrates nearly identical behavior to the NCS. Additionally, this similarity in dynamical behavior is anticipated for all small values of M to be true, perhaps fewer than M=10 but less specified.

In Section III, the time evolution of the atomic inversion for the proposed interaction system has been studied. It was found that relatively high amounts of M cause the system to become more periodic and adjust the amplitude and duration of the oscillations. On the other hand, the chosen values for M and the measured parameters make the oscillations broader or thinner. We believe this tendency towards the periodicity of revival and collapse phenomena can be useful for some applications.

In Section IV, we have investigated the nonclassical characteristics of the interaction system under study including photon statistics, normal squeezing, and amplitude-squared squeezing. It was found that the *q*-parameter temporal evolution for the selected values of M in the presence and absence of the nonlinear Kerr medium and intensity-dependent coupling is completely a sub-Poissonian statistic. Furthermore, as the amount of M increases, the *q*-parameter becomes more negative and gets closer to -1, and the fluctuations become more periodic and regular. Moreover, the study revealed that by increasing the value of M up to a certain value, the nonclassical features of the normal squeezing and the amplitude-squared squeezing occur at certain time intervals in the quadratures of $\hat{X}_1$ and $\hat{X}_2$. However, when M becomes large, these nonclassical features vanish entirely. Most importantly, it was observed that for the interaction system with the MNCSs in the presence of intensity-dependent coupling and Kerr medium, the temporal evolution of the normal and the amplitude-squared squeezing are completely

periodic in the resonance case. Compared to the linear mode, it can be concluded that the presence of χ has caused a better occurrence of these nonclassical features. In addition, the growth of M up to a certain value increases the depth of squeezing, while for a large value of M, the amount of squeezing decreases. In contrast, in the nonresonance situation, the nonclassical properties of squeezing in the quadratures of $\hat{X}_1$ and $\hat{X}_2$ occur in a brief time at the start of the interaction. This means that the existence of the detuning leads to a decrease in squeezing as a nonclassical characteristic.

Finally, in section V, to investigate the quantum entanglement of the atom and the field as a basic feature of quantum systems, we have examined the temporal evolution of the reduced entropy. We observed that when we have a nonlinear Kerr-medium and intensity-dependent coupling for resonance case, the entropy level decreases, but when the detuning is present, the entropy level increases. In all studied cases, by raising the value of M , the degree of entropy and, equivalently, the atom-field entanglement were reduced to some extent. In addition, in the nonlinear case, when the atom and the field are in the resonance the entropy of the field becomes zero at certain times of the interaction, which indicates the loss of the atom-field entanglement. In such a situation, the atom is in one of the upper or lower levels (the pure state). This is even though in other investigated cases, the degree of entropy approaches zero (not exact zero) at certain times of interaction. In our proposed system, we discovered an intriguing correlation between the purity of the field and its sub-Poissonian properties. Finally, it is necessary to note that for $f(n)=1$, the results obtained in this study are generally consistent with the results of [44] when $\chi=0$.

REFERENCES

[1] E.T. Jaynes and F.W. Cummings, "Comparison of quantum and semiclassical radiation theories with application to the beam maser," Proc. IEEE, Vol. 51, no. 1, pp. 89-109, 1963.

[2] T.R. Gentile, B.J. Hughey, D. Kleppner, and T.W. Ducas, "Experimental study of one-and two-photon Rabi oscillations," Phys. Rev. A, Vol. 40, no. 9, pp. 5103-5115, 1989.

[3] H. Moya-Cessa, V. Bužek, M. Kim, and P. Knight, "Intrinsic decoherence in the atom-field interaction," Phys. Rev. A, Vol. 48, no. 5, pp. 3900-3905, 1993.

[4] A. Joshi and M. Xiao, "Atomic-coherence effect on the Jaynes-Cummings model with atomic motion," J. Opt. Soc. Am. B, Vol. 21, no. 9, pp. 1685-1692, 2004.

[5] J.H. Eberly, N. Narozhny, and J. Sanchez-Mondragon, "Periodic spontaneous collapse and revival in a simple quantum model," Phys. Rev. Lett., Vol. 44, no. 20, pp. 1323-1326, 1980.

[6] G. Rempe, H. Walther, and N. Klein, "Observation of quantum collapse and revival in a one-atom maser," Phys. Rev. Lett., Vol. 58, no. 4, pp. 353-356, 1987.

[7] M.O. Scully and M.S. Zubairy, Quantum Optics, ed: American Association of Physics Teachers, 1999.

[8] M.S.Z.P. Meystre, "Squeezed states in the Jaynes-Cummings model," Phys. Lett. A, Vol. 89, no. 8, pp. 390-392, 1982.

[9] P. Aravind and G. Hu, "Influence of initial conditions on squeezing and anti-bunching in the Jaynes-Cummings model," Phys. B+ C, Vol. 150, no. 3, pp. 427-439, 1988.

[10] S.J. Phoenix and P. Knight, "Establishment of an entangled atom-field state in the Jaynes-Cummings model," Phys. Rev. A, Vol. 44, no. 9, pp. 6023-6029, 1991.

[11] M. Tavis and F.W. Cummings, "Exact solution for an N-molecule—radiation-field Hamiltonian," Phys. Rev., Vol. 170, no. 2, pp. 379-984, 1968.

[12] R.-h. Xie, G.-o. Xu, and D.-h. Liu, "Study of squeezing properties in a two-level system," Aust. J. Phys., Vol. 48, no. 6, pp. 907-924, 1995.

[13] P. Gora and C. Jedrzejek, "Nonlinear jaynes-cummings model," Phys. Rev. A, Vol. 45, no. 9, pp. 6816-6829, 1992.

[14] G. Agarwal and K. Tara, "Nonclassical properties of states generated by the excitations on a coherent state," Phys. Rev. A, Vol. 43, no. 1, pp. 492-497, 1991.

[15] S. Esmail, A. Salah, and S.S. Hassan, "Statistical aspects and dynamical entanglement for a two-level atom moving on along cavity length of x-direction: atomic position distribution," Braz. J. Phys., Vol. 49, pp. 438-448, 2019.

[16] A. Vaglica, "Jaynes-Cummings model with atomic position distribution," Phys. Rev. A, Vol. 52, no. 3, pp. 2319-2326, 1995.

[17] K. El Anouz, A. El Allati, A. Salah, and F. Saif, "Quantum fisher information: probe to measure fractional evolution," Int. J. Theor. Phys., Vol. 59, pp. 1460-1474, 2020.

[18] Z. M. Odibat, "Analytic study on linear systems of fractional differential equations," Comput. Math. Appl., Vol. 59, no. 3, pp. 1171-1183, 2010.

[19] N. Abdel-Wahab and A. Salah, "On the interaction between a time-dependent field and a two-level atom," Mod. Phys. Lett. A, Vol. 34, no. 10, pp. 1950081(1-16), 2019.

[20] H. Baghshahi, M. Tavassoly, and A. Behjat, "Entropy squeezing and atomic inversion in the k-photon Jaynes—Cummings model in the presence of the Stark shift and a Kerr medium: A full nonlinear approach," Chin. Phys. B, Vol. 23, no. 7, pp. 074203(1-12), 2014.

[21] B. Buck and C. Sukumar, "Exactly soluble model of atom-phonon coupling showing periodic decay and revival," Phys. Lett. A, Vol. 81, no. 2-3, pp. 132-135, 1981.

[22] M.J. Faghihi, M.K. Tavassoly, and M. Bagheri Harouni, "Tripartite entanglement dynamics and entropic squeezing of a three-level atom interacting with a bimodal cavity field," Laser Phys., Vol. 24, no. 4, pp. 045202(1-15), 2014.

[23] R. Zait, "Nonclassical statistical properties of a three-level atom interacting with a single-mode field in a Kerr medium with intensity dependent coupling," Phys. Lett. A, Vol. 319, no. 5-6, pp. 461-474, 2003.

[24] A. Othman and D. Yevick, "The interaction of a N-type four level atom with the electromagnetic field for a Kerr medium induced intensity-dependent coupling," Int. J. Theor. Phys., Vol. 57, no. 1, pp. 159-174, 2018.

[25] H. Baghshahi, M.K. Tavassoly, and A. Behjat, "Dynamics of entropy and nonclassicality features of the interaction between a◊-type four-level atom and a single-mode field in the presence of intensity-dependent coupling and kerr nonlinearity," Commun. Theor. Phys., Vol. 62, no. 3, pp. 430(1-14), 2014.

[26] G.S. Agarwal, *Quantum optics*. Cambridge University Press, 2012.

[27] R.L. de Matos Filho and W. Vogel, "Nonlinear coherent states," Phys. Rev. A, Vol. 54, no. 5, pp. 4560-4563, 1996.

[28] V. Man'ko, G. Marmo, E. Sudarshan, and F. Zaccaria, "f-Oscillators and nonlinear coherent states," Phys. Scr., Vol. 55, no. 5, pp. 528-541, 1997.

[29] J. Récamier, M. Gorayeb, W. Mochán, and J. Paz, "Nonlinear coherent states and some of their properties," Int. J. Theor. Phys., Vol. 47, pp. 673-683, 2008.

[30] A. Karimi and M.K. Tavassoly, "Quantum engineering and nonclassical properties of SU (1, 1) and SU (2) entangled nonlinear coherent states," J. Opt. Soc. Am. B, Vol. 31, no. 10, pp. 2345-2353, 2014.

[31] R. Román-Ancheyta, C. González Gutiérrez, and J. Récamier, "Photon-added nonlinear coherent states for a one-mode field in a Kerr medium," J. Opt. Soc. Am. B, Vol. 31, no. 1, pp. 38-44, 2014.

[32] F. Soto-Eguibar, B. Rodríguez-Lara, and H. Moya-Cessa, "Phase state and related nonlinear coherent states," J. Opt. Soc. Am. B, Vol. 31, no. 6, pp. 1335-1338, 2014.

[33] O. Abbasi and M.K. Tavassoly, "Superpositions of the dual family of nonlinear coherent states and their non-classical properties," Opt. Commun., Vol. 283, no. 12, pp. 2566-2574, 2010.

[34] O. Abbasi and M.K. Tavassoly, "Superposition of two nonlinear coherent states π/2 out of phase and their nonclassical properties," Opt. Commun., Vol. 282, no. 18, pp. 3737-3745, 2009.

[35] S. Sivakumar, "Studies on nonlinear coherent states," J. Opt. B: Quantum Semiclass. Opt., Vol. 2, no. 6, pp. R61-R75, 2000.

[36] O. de los Santos-Sánchez and J. Récamier, "The f-deformed Jaynes–Cummings model and its nonlinear coherent states," J. Phys. B: At. Mol. Opt. Phys., Vol. 45, no. 1, pp. 015502(1-9), 2011.

[37] O. Abbasi and A. Jafari, "Dynamics of entropy and quantum statistical properties of the field

in the interaction of a single two-level atom with a superposition of nonlinear coherent states in the framework of f-deformed Jaynes–Cummings model," Opt. Quantum Electron., Vol. 48, no. 9, pp. 1-28, 2016.

[38] O. Abbasi and A. Jafari, "Four-photon nonlinear coherent states," J. Mod. Opt., Vol. 64, no. 1, pp. 32-45, 2017.

[39] A. Othman and D. Yevick, "Quantum properties of the superposition of two nearly identical coherent states," Int. J. Theor. Phys., Vol. 57, no. 8, pp. 2293-2308, 2018.

[40] A. Dehghani, B. Mojaveri, M. Aryaie, and A. Alenabi, "Superposition of two-mode "Near" coherent states: non-classicality and entanglement," Quantum Inf. Process., Vol. 18, pp. 1-16, 2019.

[41] A. Othman, "Teleportation via the entangled derivative of coherent state," Quantum Inf. Comput., Vol. 19, no. 1&2, pp. 14-22, 2018.

[42] A. Othman, "The Mth Coherent State," Int. J. Theor. Phys., Vol. 58, no. 8, pp. 2451-2463, 2019.

[43] A.A. Othman, "Mth Coherent State Induces Patterns in the Interaction of a Two-Level Atom in the Presence of Nonlinearities," Int. J. Theor. Phys., Vol. 60, no. 4, pp. 1574-1592, 2021.

[44] S.M. Heydari, A. Jafari, and O. Abbasi, "The Mth nonlinear coherent states," Phys. Scr., Vol. 99, no. 4, pp. 045115(1-12), 2024.

[45] R. Roknizadeh and M. Tavassoly, "The construction of some important classes of generalized coherent states: the nonlinear coherent states method," J. Phys. A: Math. Gen., Vol. 37, no. 33, pp. 8111(1-18), 2004.

[46] V.I. Man'ko, G. Marmo, and F. Zaccaria, "Moyal and tomographic probability representations for f-oscillator quantum states," Phys. Scr., Vol. 81, no. 4, pp. 045004(1-7), 2010.

[47] L. Mandel and E. Wolf, *Optical coherence and quantum optics*. Cambridge university press, 1995.

[48] R. Puri and G. Agarwal, "Finite-Q cavity electrodynamics: Dynamical and statistical aspects," Phys. Rev. A, Vol. 35, no. 8, pp. 3433-3449, 1987.

[49] O. De los Santos-Sanchez and J. Récamier, "Nonlinear coherent states for nonlinear systems," J. Phys. A: Math. Theor., Vol. 44, no. 14, pp. 145307(1-18), 2011.

[50] L. Mandel, "Sub-Poissonian photon statistics in resonance fluorescence," Opt. lett., Vol. 4, no. 7, pp. 205-207, 1979.

[51] R.J. Glauber, "The quantum theory of optical coherence," Phys. Rev., Vol. 130, no. 6, pp. 25292539, 1963.

[52] C.M. Caves and B.L. Schumaker, "New formalism for two-photon quantum optics. I. Quadrature phases and squeezed states," Phys. Rev. A, Vol. 31, no. 5, pp. 3068-3092, 1985.

[53] C. Hong and L. Mandel, "Higher-order squeezing of a quantum field," Phys. Rev. Lett., Vol. 54, no. 4, pp. 323-325, 1985.

[54] M. Hillery, "Squeezing of the square of the field amplitude in second harmonic generation," Opt. Commun., Vol. 62, no. 2, pp. 135-138, 1987.

[55] C.H. Bennett, "Quantum information and computation," Phys. Today, Vol. 48, no. 10, pp. 24-30, 1995.

[56] C.H. Bennett and D.P. DiVincenzo, "Quantum information and computation," Nature, Vol. 404, no. 6775, pp. 247-255, 2000.

[57] R. Naderali, H. Motiei, and A. Jafari, "Creation of entangled W states of four two-level atoms in a cavity via quadrapod adiabatic passage," Opt. Quantum Electron., Vol. 45, pp. 97-103, 2013.

[58] G. Alber Alber, T. Beth, M. Horodecki, P. Horodecki, R. Horodecki, M. Rötteler, H. Weinfurter, R. Werner, and A. Zeilinger, *Quantum information: An introduction to basic theoretical concepts and experiments*. Springer, 2003.

[59] A. Mortezapour, M. Mahmoudi, and M. Khajehpour, "Atom–photon, two-mode entanglement and two-mode squeezing in the presence of cross-Kerr nonlinearity," Opt. Quantum Electron., Vol. 47, no. 7, pp. 2311-2329, 2015.

[60] A. Wehrl, "General properties of entropy," Rev. Mod. Phys., Vol. 50, no. 2, pp. 221-260, 1978.

[61] H. Araki and E.H. Lieb, "Entropy inequalities," Commun. Math. Phys., Vol. 18, no. 2, pp. 160-170, 1970.

[62] A. Vidiella-Barranco, H. Moya-Cessa, and V. Bužek, "Interaction of Superpositions of Coherent States of Light with Two-level Atoms," J. Mod. Opt., Vol. 39, no. 7, pp. 1441-1459, 1992.

Seyyed Majid Heydari was born in Maragheh, East Azarbaijan, Iran, in 1986. He obtained his Bachelor of Science degree in Solid-State Physics from Payam Noor Bonab branch in 2011 and his Master of Science degree in Atomic and Molecular Physics from Urmia University in 2015. He is currently a Ph.D. candidate in optics and lasers in Urmia University. His research interests include quantum optics, nonlinear optics and generalized coherent states.

Akbar Jafari is a professor of physics in the Department of Physics, Urmia University, Urmia, Iran. He is a member of the Iranian Society of Physics, Iranian Society of Optics and Photonics. Linear and nonlinear optics, nonlinear optical properties of nematic liquid crystals, and laser dynamics are some of his research interests.

Omid Abbasi is assistant professor in the department of physics, faculty of computer engineering, Azad University of Najafabad, Iran. He received his PhD in physics in the general field of quantum optics from Urmia University in 2016. Quantum optics and quantum information are some of his research interests.